2878 *J. Phys. Chem. A* **2005,** *109,* 2878−2886

DFT/TDDFT Studies of the Geometry, Electronic Structure and Spectra of (12S)-1,4,7,10-Tetraazadicyclo[10,3,0]-pentadecane-3,11-dione and Its Derivatives

Wei Li,[†] Yi-Bo Wang,[‡] Ioana Pavel,[§] Quan Yuan,[†] Yong Ye,[†] En-Qin Fu,[†] Ming-Dao Luo,[†] Ji-Ming Hu,*,[†,§] and Wolfgang Kiefer[§]

College of Chemistry and Molecular Sciences, Wuhan University, Wuhan 430072, P.R. of China, Department of Chemistry, Guizhou University, Guiyang, Guizhou 550025, P.R of China, and Institut für Physikalische Chemie, Universität Würzburg, Am Hubland, D-97074 Würzburg, Germany

Received: August 15, 2004; In Final Form: January 29, 2005

The FT-Raman and UV−visible spectra of (12S)-1,4,7,10-tetraazadicyclo[10,3,0]-pentadecane-3,11-dione and its derivatives were obtained and discussed. The harmonic vibrational wavenumbers and the corresponding Raman scattering activities in their electronic ground-states were calculated at the DFT-B3LYP/6-31G(d) level of theory. The calculated wavenumbers were then scaled and compared with the experimental values. The 7-(2,4-dinitrophenyl)-(12S)-1,4,7,10-tetrazadicyclo[10,3,0]-pentadecane-3,11-dione derivative has mainly an amide (II) character, while the others have an amide (I) character. Moreover, the different substituents do not cause a significant shift of the vibrational mode of the macrocyclic plane. The electronic vertical excitation energy and the oscillator strength were determined with the help of TDDFT calculations and by employing pure (BLYP) and hybrid (B3LYP, B3P86, and *m*PW1PW91) functionals together with the 6-31G(d) basis set. The BLYP functional reproduces the UV−vis absorption spectra better than the B3LYP, B3P86, or *m*PW1PW91 hybrid functionals. A dimolecular model, which considers hydrogen-bonded structures, proved that strong inter- and intramolecular hydrogen bonds are present in these compounds. Due to the transannular effect, the UV−vis absorption spectrum of macrocyclic dioxotetraamines is completely different from that of single amide compounds.

1. Introduction

The structures and properties of macrocyclic dioxotetraamines are similar to those of the tripeptide. They are capable of coordinating to a divalent 3d cation with simultaneous extrusion of two hydrogen ions from the amido groups.[1−2] Moreover, transition metal (II) complexes of macrocyclic dioxotetraamines are known to have interesting properties and important biological functions (e.g., models for metalloproteins and oxygen carriers).[3,4] Copper(II) and zinc(II) complexes of dioxotetraamine ligands are able to identify small molecules[5] and can also be used as metal enzyme models with physiological activity.[6]

The study of macrocyclic polyamines has been an active area of research with remarkable achievements. New synthetic routes and the effect of the functional pendant arms on the properties of 13-membered macrocyclic dioxotetraamine ligands, as well as their crystal structures, have been constantly investigated and reported.[7−10] The fluorescence and UV−vis absorption spectra of 1,4,7,10-tetraazacyclotridecane-11,13-dionato and its Cu(II), Co(II), Ni(II) complexes as mimic superoxide dismutase metalloenzymes were also measured at different pH values. The correspondence between their catalytic activities and the character of the fluorescence spectra was also analyzed.[11,12] Analogously, the UV−vis absorption spectra of the Cu(III) and Ni(III) complexes with open-chain and the macrocyclic ligands containing two amide and two amine groups were recorded and assigned.[13] The equilibrium and the kinetic of copper(II) and mercury(II) complex formation of 13−15- and 16−18-membered macrocyclic dioxotetraamines have been also explored.[14−15]

Time-dependent density functional theory (TDDFT), found in 1984 by Runge and Gross,[16] can be viewed as an exact reformulation of the time-dependent quantum mechanics, where the fundamental variable is no longer the many-body wave function but the density. More recently, a number of papers have shown that the TDDFT approach offers an efficient alternative to the high-level ab initio techniques for providing sound excitation energies and achieves a reasonable accuracy in the calculation of excitation energies at a low computation cost.[17−20]

Raman spectroscopy has extensively been used as a tool for the qualitative and quantitative analysis and for the structure determination of new compounds. Therefore, the combination of theoretical calculations and spectroscopy should give a comprehensive understanding of the structure of new compounds, for which single crystal synthesis is extremely difficult.

We present here for the first time the UV−vis and FT-Raman spectra of (12S)-1,4,7,10-tetraazadicyclo[10,3,0]-pentadecane-3,11-dione (**a**), and its derivatives: 7-(2,4-dinitrophenyl)−(12S)-1,4,7,10-tetrazadicyclo[10,3,0]-pentadecane-3,11-dione (**b**), 7-benzyl-(12S)-1,4,7,10-tetraazadicyclo[10,3,0]-pentadecane-3,11-dione (**c**), (2S)-2-benzyl-1,4,7,10-tetraazadodecane-3,11-dione(**d**), and (2S)-2-isopropyl-1,4,7,10-tetraazadodecane-3, 11-dione (**e**), respectively.

Their electronic vertical excitation energies and oscillator strengths were determined with the help of TDDFT calculations and by employing pure (BLYP) and hybrid (B3LYP, B3P86

---

* Corresponding author. E-mail: jmhu@whu.edu.cn; Fax:+86-027-68757617.

[†] Wuhan University.

[‡] Guizhou University.

[§] Universität Würzburg.

10.1021/jp0463262 CCC: $30.25

TABLE 1: Selected Bond Lengths and Dihedral Angles of Compounds a, b, c, d, and e Calculated at the B3LYP/6-31G(d) Level

compounds	a	b	c	d	e	dimer of **e**	X-ray[a]
				Bond Distances (Å)			
N1−C1	1.480	1.493	1.491	1.470	1.474	1.460(1.470)	
C1−C2	1.530	1.530	1.530	1.552	1.550	1.550 (1.550)	1.524(12)
C2−N2	1.360	1.370	1.360	1.360	1.350	1.350 (1.350)	1.318(12)
N2−C3	1.460	1.450	1.450	1.460	1.460	1.460 (1.460)	1.470(12)
C3−C4	1.530	1.540	1.540	1.550	1.530	1.530 (1.530)	1.510(15)
N3−C4	1.460	1.460	1.450	1.440	1.450	1.450 (1.450)	1.472(12)
N3−C5	1.440	1.460	1.450	1.450	1.460	1.460 (1.460)	1.472(13)
C5−C6	1.550	1.540	1.540	1.530	1.540	1.530 (1.530)	1.519(14)
C6−N4	1.450	1.450	1.450	1.460	1.450	1.460 (1.460)	1.444(12)
N4−C7	1.360	1.360	1.350	1.360	1.350	1.340 (1.340)	1.304(12)
C7−C8	1.530	1.530	1.530	1.530	1.540	1.530 (1.530)	1.516(12)
C8−N1	1.455	1.460	1.480	1.450	1.460	1.460 (1.460)	
C2−O1	1.230	1.220	1.220	1.220	1.230	1.230 (1.230)	1.247(11)
C7−O2	1.220	1.220	1.220	1.220	1.220	1.220 (1.230)	1.254(10)
O1−H1				2.380			
O1−H2		2.360					
O1−H3				2.140	2.230	2.150(2.190)	
O1−H4						2.300(2.490)	
O2−H3	2.100						
O2−H2′[b]						1.970	
				Dihedral angles (deg.)			
N1−C1−C2−N2	−103.5	127.2	90.1	−78.9	98.5	94.5 (104.7)	
N2−C3−C4−N3	73.0	63.5	−60.9	−47.8	−73.3	−74.1 (−70.8)	
N3−C5−C6−N4	49.1	−42.0	−43.1	−71.1	53.7	55.1 (57.1)	
N4−C7−C8−N1	−44.7	−8.0	−4.1	153.0	13.0	2.8 (10.0)	

[a] The X-ray crystal structure of Cu(II) 4,7-bis(2-methylfuran)-1,4,7,10-tetraazacyclotridecane-11,12-dione.[8] [b] The intermolecular O−H distance.

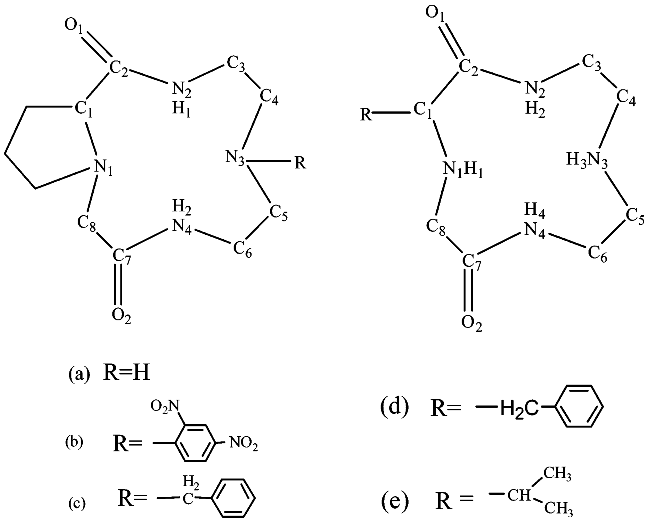

Figure 1. Atom numbering and structures of compounds **a**, **b**, **c**, **d**, and **e**.

and *m*PW1PW91) functionals together with the 6-31G(d) basis set. The harmonic vibrational wavenumbers and the corresponding Raman scattering activities for their electronic ground-states were then obtained at the B3LYP/6-31G(d) level of theory. The aim of the present work is to provide a sound assignment for their vibrational and UV−visible spectra and to estimate the excitation energies and the oscillator strength of (12S)-1,4,7,-10-tetraazadicyclo[10,3,0]-pentadecane-3,11-dione and its derivatives.

2. Experimental and Computational Methods

Samples were synthesized according to the literature[21,22] and dissolved in dichloromethane. A Perkin-Elmer UV−vis−NIR spectrometer (model Lambda 19) was used to record the absorption spectra. The FT-Raman spectra of the solid samples (powders) were recorded with a Brucker spectrometer (model IFS 120HR) equipped with an integrated FRA 106 Raman module. The 1064 nm radiation from a Nd:YAG laser with an output of about 300 mW was used for excitation. The spectral range of interest was 100−3700 cm^{-1}.

Geometries of the compounds were optimized by performing DFT calculations at the B3LYP/6-31G(d) level of theory. Structures obtained have C_1 symmetry (Figure 1). Afterward, the vibrational wavenumbers were obtained at the same level of theory by using the optimized geometries. The vertical excitation energies and the oscillator strengths were determined with the help of TDDFT calculations and by employing pure (BLYP) and hybrid (B3LYP, B3P86, and *m*PW1PW91) functionals together with the 6-31G(d) basis set (for the B3LYP/6-31G(d) optimized structure).

The 6-31G(d) basis set employed in the TDDFT calculations led to good results for the these compounds. Moreover, the B3LYP/6-31G(d) approach was found to be reliable for predicting the vibrational modes and their relative Raman intensity in electronic ground states.

All calculations were carried out using the Gaussian 98 program[23] on an Alpha 21164/433 au workstation of GHPCC of the Guizhou University.

3. Results and Discussion

3.1. Geometry. The structure of the investigated compounds is presented in Figure 1 and their calculated structural parameters along with the X-ray crystal values for Cu(II) complex of 4,7-bis(2-methylfuran)-1,4,7,10-tetraazacyclotridecane-11,12-dione are listed in Table 1.

One can notice that the different substitutents of the C1 and N3 atoms do not change the bond lengths significantly but affect the dihedral angles. The bond lengths of compounds **a**, **b**, **c**, **d**, and **e** as well as the dimer of compound **e** are within about 0.02 Å. The comparison between the calculated bond lengths for compounds **a**, **b**, **c**, **d**, **e** and the experimental values of Cu(II) complex of 4,7-bis(2-methylfuran)-1,4,7,10-tetraazacyclo-

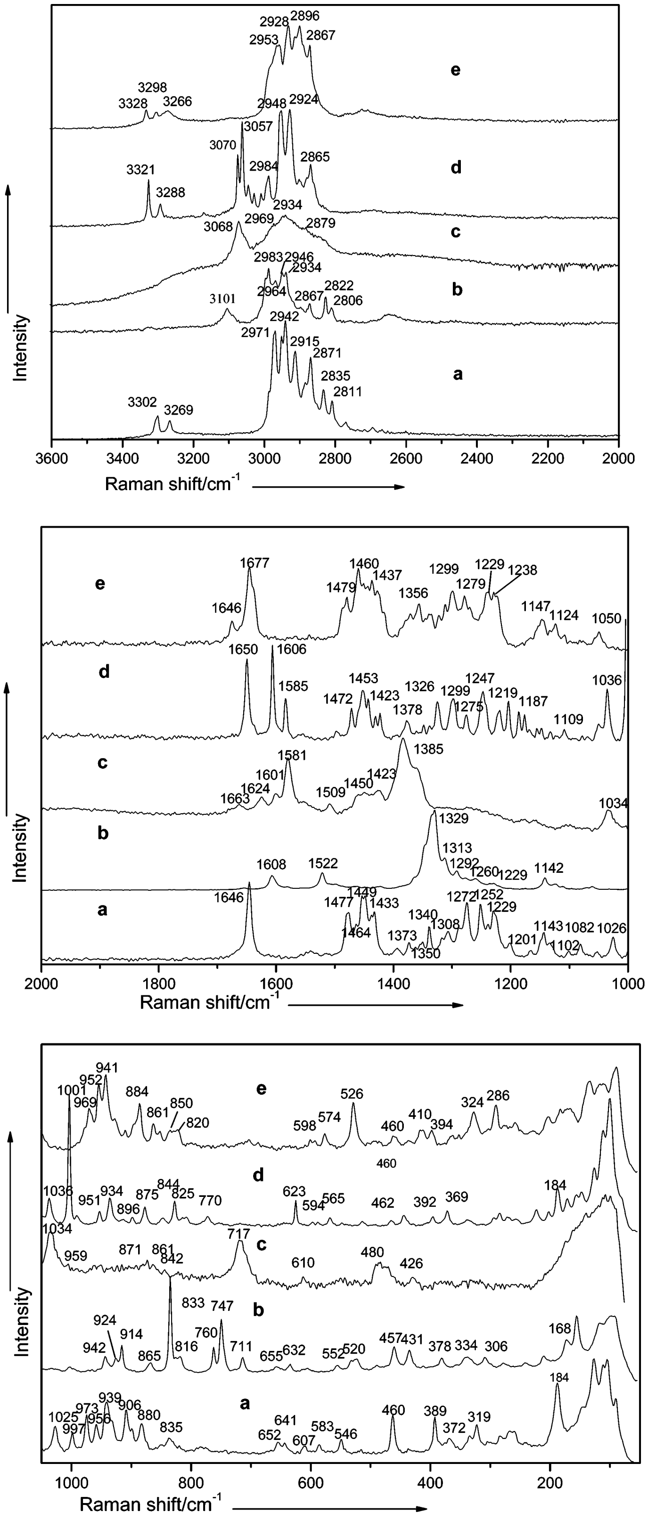

Figure 2. The FT-Raman spectra of compounds **a**, **b**, **c**, **d**, and **e**.

tridecane-11,12-dione indicate a deviation of about 0.02−0.04 Å. This is due to structural differences and the approximations used in the functional and basis set employed in the calculations. Because of the steric effect, the frames of the macrocyclic multiamine have to be twisted in order to reduce the potential energy.

3.2. Vibrational Spectra. The FT-Raman spectra of **a**, **b**, **c**, **d**, and **e** are shown in Figure 2. The observed and calculated wavenumbers along with their corresponding Raman scattering activities are included in Table 2. All calculated harmonic wavenumbers were scaled by a common (for this level of theory) factor of 0.9614,[24] excepting the ν(N−H) and ν(C−H) modes. Due to their more anharmonic character, smaller scaling factors of 0.922 and 0.954 had to be used for their calibration. For comparison reasons, the calculated spectra were simulated by using a Gaussian function and inserted in Figure 3 along with the experimental spectra. The full width at half-maximum of each peak (fwhm) is 8 cm^{-1} and the spectral range is between 3500 and 0 cm^{-1}.

The compounds **a**, **b**, **c**, **d**, and **e** have 105, 147, 144, 123, and 111 vibrational modes, respectively. The discrepancies between the calculated and experimental values were mostly smaller than 30 cm^{-1}. A significant error appeared for the ν(C═O) mode. The fundamentals can be observed at 1677−1663 cm^{-1} and 1654−1624 cm^{-1}, while the calculated modes were determined at 1712.4−1711.3 cm^{-1} and 1705.6−1688.7 cm^{-1}, respectively. Such large errors may be due to the existence of the amide in dimer or polymer forms in solid state. Accordingly, the intra- and intermolecular hydrogen bonds cause a significant shift of the ν(C═O) and ν(N−H) modes to lower wavenumbers. However, one should take into account that the theoretical calculations refer to a single molecule in vacuum, which probably does not describe the real environment the best.

To solve this problem, the geometry of the dimer of compound **e** was optimized at the B3LYP/6-31G(d) level by considering hydrogen bonded structures. Its harmonic vibrational modes were also determined using the same method. The calculated structural parameters are inserted in Table 1. The scaled wavenumbers, their Raman scattering activities, and the proposed assignments are presented in Table 3.

One can notice from Table 1 that the intramolecular O−H distance of amide is about 2.150−2.490 Å, while the intermolecular O−H distance of amide is approximately 1.970 Å. Such short atom−atom distances reflect the existence of strong inter- and intramolecular hydrogen bonds. Analogously, from Table 3 one can observe that the calculated wavenumbers of the ν(C═O) mode at 1675.7 and 1653.4 cm^{-1} are very close to the experimental fundamentals at 1677 and 1646 cm^{-1}, respectively. Therefore, the inter- and intramolecular hydrogen bonds are indeed the main cause of the significant discrepancy between the experimental and theoretical values.

The FT-Raman spectra of compounds **a**, **c**, **d**, and **e** show far-reaching similarities for most of the band patterns. However, some differences appear in the position and the relative intensity of a few peaks. The ν(N−H) modes appear at 3328−3302 cm^{-1} and 3298−3266 cm^{-1}, while the ν(C═O) modes can be observed between 1677 and 1624 cm^{-1}. They represent the characteristic bands of amide (I). There are no peaks in these two spectral regions for compound **b**. Nevertheless, the medium band at 1522 cm^{-1} was assigned to the δ(N−H) vibration. Therefore, compounds **a**, **c**, **d**, and **e** have mainly amide (I) character, while **b** has an amide (II) character. The peaks at 3101cm^{-1} and 3070−3024 cm^{-1} can be attributed to the ν(C−H) mode of phenyl. The corresponding ν(C−C) modes were observed at 1608−1601, 1585−1581, and 1509−1497 cm^{-1}, respectively. The breathing vibration of the single-substituted benzene ring appears at 1001 cm^{-1}. Analogously, the δ(C−H) and γ(C−H) modes of the benzene ring occur at 1148−1124, 865−861, 747−652, 602−598, and 552−526 cm^{-1}, respectively. The very strong band at 1329 cm^{-1} in the Raman spectrum of **b** was attributed to the symmetric stretching vibration of nitryl. Its asymmetric mode could not be detected.

The bands at 1477−1423 cm^{-1} were assigned to the δ(CH$_2$) mode. The in-plane wagging and twisting vibrations of methylene were observed at 1385−1372, 1356−1299, and 1279−

TABLE 2: Observed Fundamentals and Scaled Wavenumbers (cm^{-1}) along with Raman Scattering Activities (values in square brackets in Å^4/amu)[a]

assignment	a		b		c		d		e	
	calc.[b]	exp.	calc.	exp.	calc.	exp.	calc.	exp.	calc.	exp.
ν(N−H)	3301.6 [47.4]	3302					3335.0 [50.8]	3321	3339.1[39.6]	3328
ν(N−H)	3258.7 [51.0]	3269					3266.3 [39.8]	3288	3280.8[35.4]	3298
ν(N−H)									3274.5[135.8]	3266
ν(C−H)$_{\mathrm{ben}}$			3091.0[103.8]	3101			3061.0 [319.9]	3070		
ν(C−H)$_{\mathrm{ben}}$					3058.8[327.0]	3068	3043.7 [105.3]	3057		
ν(C−H)$_{\mathrm{ben}}$							3034.1 [81.3]	3041		
ν(C−H)$_{\mathrm{ben}}$							3027.1 [32.1]	3024		
ν_{a}(CH3)									2969.4[111.2]	2960
ν_{a}(CH2)	2969.3 [145.8]	2971	2975.4[148.9]	2983	2964.9[90.1]	2969	2993.6 [54.8]	2984		
ν_{a}(CH2)	2943.8 [165.9]	2942	2935.8 [144.9]	2946	2943.6[133.4]	2934	2950.5 [53.4]	2948	2948.7[80.2]	2953
ν_{a}(CH2)	2924.4 [75.4]	2915					2938.7 [167.2]	2924	2919.3[152.7]	2928
ν_{s}(CH2)	2892.8[289.9]	2887	2895.5 [245.8]	2893	2907.1[133.1]	2879	2899.7[182.3]	2897	2899.8[98.7]	2896
ν_{s}(CH2)	2875.5 [126.5]	2871					2854.5 [173.5]	2865	2858.3[221.2]	2867
ν_{s}(CH2)	2855.3 [108.1]	2835	2867.7[67.0]	2822						
ν_{s}(CH2)	2805.5 [38.0]	2811								
ν(C=O)					1712.4[7.1]	1663			1711.3[2.4]	1677
ν(C=O)	1690.7 [6.7]	1646	1688.7 [7.7]	1654	1705.6[1.7]	1624	1695.3 [2.1]	1650	1689.6[4.1]	1646
ν(C=C)$_{\mathrm{ben}}$			1601.8[10.8]	1608	1598.6[40.8]	1601	1601.8 [45.3]	1606		
ν(C=C)$_{\mathrm{ben}}$			1594.9[119.9]	1582	1578.7[10.1]	1581	1582.2 [8.9]	1585		
δ(N−H)			1514.9[4.6]	1522						
ν(C=C)$_{\mathrm{ben}}$					1516.4[8.4]	1509	1493.2[4.6]	1497		
δ_{as}(CH3)									1476.3[35.4]	1479
δ_{as}(CH3)									1466.6[16.8]	1460
δ(CH2)	1469.7 [16.1]	1477					1481.3 [8.9]	1472		
δ(CH2)	1461.0[19.3]	1464	1457.6[21.9]	1461	1462.5[17.3]	1460	1455.9 [12.6]	1453	1450.4[7.8]	1451
δ(CH2)	1449.9 [19.6]	1449	1455.2[16.5]	1449	1441.4[13.6]	1450	1448.2 [12.9]	1444	1446.8[16.9]	1444
δ(CH2)	1443.9 [14.8]	1433			1429.8[9.9]	1423	1443.5 [15.2]	1431	1440.7[13.3]	1437
δ(CH2)			1432.8[17.8]	1423			1437.3[10.6]	1423	1431.7[8.4]	1428
ω(CH2)+τ(CH2)	1366.0 [4.8]	1373	1369.2[27.6]	1365	1361.4[16.9]	1385	1364.9 [9.2]	1378	1373.9[6.7]	1372
ν_{s}(NO2)			1339.2[303.4]	1329						
ω(CH2)+τ(CH2)	1353.9[4.88]	1350					1358.1[14.2]	1349	1362.1[9.8]	1356
ω(CH2)+τ(CH2)	1346.0 [4.4]	1340					1329.5 [19.0]	1326	1350.1[12.6]	1340
ω(CH2)+τ(CH2)	1323.2[4.6]	1308	1334.2[43.8]	1313			1291.1[10.5]	1299	1284.6[13.5]	1299
ν_{ske} of ben ring			1304.9[21.6]	1292						
ω(CH2)+τ(CH2)	1256.5 [12.8]	1275	1262.8[4.9]	1278	1277.8[10.2]	1275	1259.6 [14.3]	1275	1266.9[16.2]	1279
ω(CH2)+τ(CH2)	1247.4 [23.9]	1252	1257.4[7.5]	1260	1251.4[14.4]	1243	1237.6 [11.0]	1247	1243.6[7.4]	1238
ω(CH2)+τ(CH2)	1240.4 [8.1]	1229	1242.2[20.7]	1229			1223.1 [6.4]	1219	1229.7[4.3]	1229
ν_{as}(C−N−C)	1207.5[5.1]	1201					1186.5[19.0]	1187		
ν_{as}(C−N−C)	1186.6[6.4]	1165			1171.9[18.2]	1175	1181.6[6.8]	1177		
ν_{as}(C−N−C)	1171.2 [15.1]	1143	1144.8[3.3]	1142	1167.8[9.9]	1161	1152.5 [2.7]	1156	1149.4[3.9]	1147
δ(C−H)$_{\mathrm{ben}}$			1123.1[93.1]	1124			1146.7[5.1]	1148		
υ_{as}(C−N−C)	1119.0[3.2]	1134							1127.3[3.6]	1124
ν_{as}(C−N−C)	1097.7[4.1]	1102	1105.3[8.7]	1111			1112.3[4.7]	1109	1110.7[1.5]	1109
ν_{s}(C−N−C)	1087.1[3.4]	1082	1099.6[6.2]	1070						
ν_{s}(C−N−C)	1064.5 [5.5]	1052	1075.1[4.8]	1061			1062.6 [2.2]	1050	1055.7[1.5]	1050
ν_{s}(C−N−C)	1038.6 [3.0]	1025			1037.8[10.8]	1034	1020.9 [3.4]	1036		
breath of five-member ring	1002.8[8.2]	997								
breath of ben ring							979.6[30.5]	1001		
ν(C−C)	977.2[1.4]	973							945.1[4.0]	969
ν(C−C)	947.4 [1.0]	956	936.0[7.4]	942	979.2[28.9]	959	960.0 [4.2]	951	943.4[6.8]	952
ν(C−C)	917.6 [4.6]	939	936.0[7.4]	924	959.4[5.5]	948	919.9 [5.3]	934	923.9[4.3]	941
ν(C−C)	906.2[4.8]	906	910.9[5.1]	914			895.8[0.5]	896	892.9[3.8]	907
ρ(CH2) +υ(C−C)	863.9 [3.2]	880			871.5[9.3]	871	882.4 [4.1]	875	881.3[5.3]	884
γ(C−H)$_{\mathrm{ben}}$			852.6[2.7]	865	865.1[1.3]	861				
ν(C−C)									861.6[1.7]	861
ρ(CH2)+ ν(C−C)	843.0 [0.6]	835			829.4[4.8]	842	849.8[5.7]	844	844.8[3.7]	850
ν(C−NO2)			811.5[20.1]	833						
ρ(CH2)+ ν(C−C)	804.4[6.2]	818			812.5[11.6]	819	816.1[11.1]	825	803.3[8.2]	820
ρ(CH2)+ ν(C−C)	792.8[8.5]	783	781.6[8.8]	760			768.2 [2.2]	770		
γ(C−H)$_{\mathrm{ben}}$			756.1[10.7]	747						
γ(C−H)$_{\mathrm{ben}}$			704.9[1.1]	711	712.0[10.8]	717				
γ(N−H)	673.6[1.6]	652	638.2[6.3]	655						
in-plane def of ring	623.2[2.0]	641								
in-plane def of benzene ring			625.4[4.4]	632	612.3[4.5]	610	612.5 [4.8]	623		
γ(N−H)	581.9[1.0]	607	590.0[2.3]	602			589.3[0.5]	594	620.5[2.7]	598
In-plane def of ring	564.4[1.7]	583					555.7[2.2]	565	569.3[1.0]	574
γ(N−H)	531.7[0.6]	546	540.8[2.1]	552					503.8[3.0]	526
out-of-plane def of ben ring			534.9[0.8]	520						
δ(C−N−C)	486.6 [1.3]	460	455.1[7.5]	457	508.3[2.7]	480			468.4[1.9]	460
out-of-plane def of ben ring			426.9[7.2]	431	470.7[3.7]	467	451.2 [1.4]	462		
δ(C−N−C)					445.3[2.8]	426			422.1[1.4]	410
δ(C−N−C)	367.4 [3.5]	389					410.4 [2.9]	392	393.6[1.8]	394
out-of-plane def of ring	352.9[2.3]	372					397.3[1.1]	369	356.7[1.2]	360
out-of-plane def of ben ring			375.7[3.0]	378						
tilt of N−C−C−N	311.8[1.4]	319	292.0[2.3]	306			326.7[1.5]	335	327.7[1.6]	324
tilt of N−C−C−N	275.6[0.5]	263					266.8[1.3]	267	295.7[0.7]	286
tilt of N−C−C−N	193.5[1.1]	184					207.1[0.9]	184	159.6[0.5]	179

[a] ν stretching; δ bending; τ torsion; γ out-of-plane wagging; ω in-plane wagging; a asymmetric; s symmetric; ben, benzene ring; skel, skeleton.

[b] B3LYP/6-31G(d) scaling factor: 0.9614 with the exception of ν(N−H):0.922; ν(C−H):0.954.

TABLE 3: Observed Fundamentals and Scaled Wavenumbers (cm^{-1}) along with Raman Scattering Activities (values in square brackets in Å^4/amu) of Dimer of Compound e[a]

assignment	exp.	freq[b]	Raman intensity	assignment	exp.	freq	Raman intensity
ν(N−H)	3328	3310.2	50.7	ν_{as}(C−N−C)	1147	1151.1	5.0
ν(N−H)	3298	3287.8	73.6	ν_{as}(C−N−C)	1124	1130.8	3.1
ν(N−H)	3266	3239.6	289.0	ν_{as}(C−N−C)	1109	1094.5	3.1
ν_{a}(CH2)	2960	2968.5	130.2	ν_{s}(C−N−C)	1050	1066.6	2.2
ν_{a}(CH2)	2953	2933.9	161.1	ν(C−C)	969	951.1	5.5
ν_{a}(CH2)	2928	2909.2	177.1	ν(C−C)	952	944.4	3.7
ν_{s}(CH2)	2896	2896.0	112.1	ν(C−C)	941	925.9	6.2
ν_{s}(CH2)	2867	2855.1	222.7	ν(C−C)	907	897.2	5.7
ν(C=O)	1677	1675.7	10.4	ρ(CH2) +ν(C−C)	884	884.2	7.8
ν(C=O)	1646	1653.4	13.2	ν(C−C)	861	862.6	1.6
δ_{as}(CH3)	1479	1476.3	38.2	ρ(CH2)+ ν(C−C)	850	845.4	3.7
δ_{as}(CH3)	1460	1466.6	15.9	ρ(CH2)+ ν(C−C)	820	801.6	9.4
δ(CH2)	1451	1458.4	10.8	γ(N−H)	598	606.8	3.6
δ(CH2)	1444	1443.7	12.5	in-plane def of ring	574	579.3	3.1
δ(CH2)	1437	1440.4	15.4	γ(N−H)	526	517.4	3.5
δ(CH2)	1428	1425.0	14.3	δ(C−N−C)	460	470.5	2.7
ω(CH2)+τ(CH2)	1372	1363.7	9.5	δ(C−N−C)	410	428.1	1.6
ω(CH2)+τ(CH2)	1356	1351.8	20.1	δ(C−N−C)	394	398.3	2.0
ω(CH2)+τ(CH2)	1340	1331.9	9.5	out-of-plane def of ring	360	354.3	1.9
ω(CH2)+τ(CH2)	1299	1285.9	17.7	tilt of N−C−C−N	324	328.6	1.4
ω(CH2)+τ(CH2)	1279	1272.6	12.5	Tilt of N−C−C−N	286	247.6	1.5
ω(CH2)+τ(CH2)	1238	1231.6	8.3	Tilt of N−C−C−N	179	153.8	1.5
ω(CH2)+τ(CH2)	1229	1212.8	10.3				

[a] ν stretching; δ bending; τ torsion; γ out-of-plane wagging; ω in-plane wagging; a asymmetric; s symmetric; def, deformation. [b] B3LYP/6-31G(d) scaling factor: 0.9614 with the exception of ν(N−H):0.922; ν(C−H):0.954.

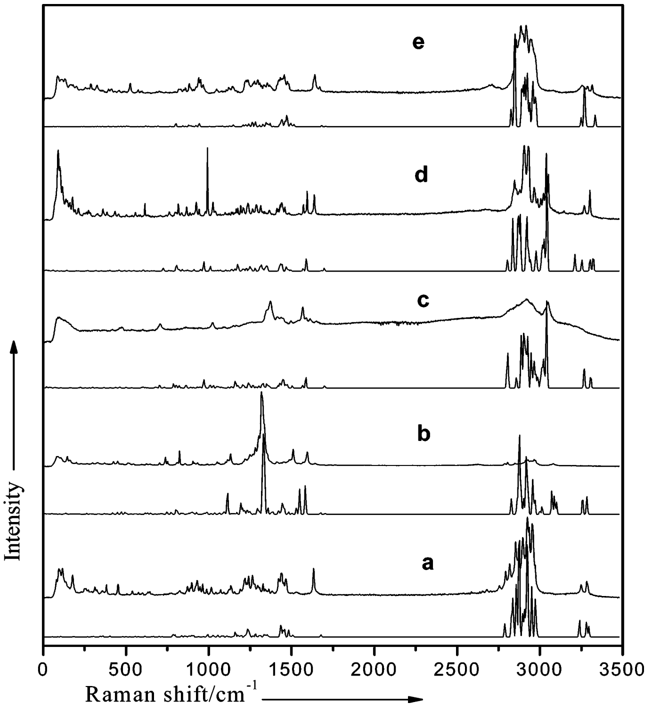

Figure 3. Comparison between the experimental and simulated theoretical spectra (upper is experimental spectra, lower is the simulated spectra).

1219 cm^{-1}, respectively. The asymmetric C−N−C stretching vibrations appear at 1201−1142 cm^{-1} and 1134−1102 cm^{-1}, and the corresponding symmetric stretching mode occurs at 1082−1025 cm^{-1}. The carbon link stretching vibration was detected at 973−896 cm^{-1}. The out-of-plane wagging of methylene couples with the C−C stretching vibration and gives rise to the peaks at 884−871, 861, 850−835, 825−818, and 783−760 cm^{-1}, respectively. Analogously, the C−N−C bending vibrations appear at 480−460 cm^{-1} and 426−389 cm^{-1}. Moreover, the breathing vibration of the five-member ring was observed at 997 cm^{-1} and the in-plane vibrations of the macrocycle were ascribed at 641 cm^{-1} and 583−565 cm^{-1}, respectively. The bands below 400 cm^{-1} are due to C−C−C or C−N−C bending and torsion modes. It should also be mentioned that the different substituents at C1 and N3 do not cause a significant shift of the vibrational mode of the macrocyclic plane.

3.3. Electronic Spectra. The energy levels of the frontier orbital of compounds **a**, **b**, **c**, **d**, and **e** obtained at the B3LYP/6-31G(d) level of theory are listed in Table 3. The energy level of the highest occupied molecular orbital (E_{HOMO}) and of the lowest unoccupied molecular orbital (E_{LUMO}) of compound **b** is about 0.5−0.7 and 2.7−2.9 eV, respectively, lower than those of the other compounds. As a result, the $E_{\mathrm{HOMO}}-E_{\mathrm{LUMO}}$ gap in compound **b** is about 2.0 eV smaller than those in the compounds **a**, **c**, **d**, and **e**, respectively. Moreover, the energetic gaps between some orbitals in compounds **b** and **c** are diminished to be degenerate. The two highest occupied molecular orbitals have in all compounds a major contribution from the lone pair electrons of the N or O atoms. Analogously, the two lowest unoccupied molecular orbitals have mostly an antibonding π character.

The UV−vis absorption spectra of compounds **a**, **b**, **c**, **d**, and **e** are listed in Figure 4. The comparison of the UV−vis absorption spectra of compounds **a**, **b**, **c**, **d**, and **e** reveals a strong band located at almost the same place in all spectra (near 226 nm). One can also notice a medium or weak broad peak at higher wavelengths for compounds **b** and **c**, respectively. To estimate the excitation energies and the oscillator strengths as well as to verify the method of dependence (which employed different xc potentials), various TDDFT calculations have been performed on the mentioned compounds. We have also compared the experimental data with the theoretical results, which allowed us to establish the best approach and to identify the trends. All data are listed in Tables 5−9. In fact, the different xc potentials influence the excitation energy and the oscillator strengths significantly. The B3LYP and B3P86 hybrid functionals present a similar behavior as regards the excitation

TABLE 4: Frontier Orbital Energy Levels of Compounds (in eV) Calculated at B3LYP/6-31G(d) Level of Theory

orbitals	**a**	**b**	**c**	**d**	**e**
HOMO-8	−9.548 (σ)	−8.053 (π)	−7.352 (π)	−9.131 (π)	−9.464 (σ)
HOMO-7	−9.351 (π)	−8.009 (π)	−7.266 (n)	−7.470 (n)	−9.245 (π)
HOMO-6	−9.192 (π)	−7.758 (π)	−6.700 (n)	−7.359 (n)	−9.064 (π)
HOMO-5	−7.148 (n)	−7.533 (n)	−6.683 (π)	−6.994 (π)	−7.238 (n)
HOMO-4	−6.973 (n)	−7.253 (n)	−6.657 (π)	−6.904 (n)	−7.137 (n)
HOMO-3	−6.848 (n)	−7.116 (n)	−6.519 (π)	−6.709 (π)	−6.818 (n)
HOMO-2	−6.748 (n)	−6.848 (n)	−6.470 (π)	−6.511 (π)	−6.577 (n)
HOMO-1	−6.010 (n)	−6.478 (n)	−5.598 (n)	−5.878 (n)	−6.104 (n)
HOMO	−5.501 (n)	−6.110 (n)	−5.364 (n)	−5.538 (n)	−5.358 (n)
LUMO	0.273 (π*)	−2.698 (π*)	0.016 (π*)	−0.020 (π*)	0.183 (π*)
LUMO+1	0.747 (π*)	−2.442 (π*)	0.061 (π*)	0.072 (π*)	0.991 (π*)
LUMO+2	1.884 (π*)	−0.787 (π*)	0.078 (π*)	0.309 (π*)	1.265 (π*)
LUMO+3	2.346 (π*)	−0.169 (π*)	0.731 (π*)	0.701 (π*)	1.944 (π*)
LUMO+4	2.445 (σ*)	−0.107 (π*)	1.431 (π*)	1.007 (π*)	2.738 (σ*)

energy, the oscillator strengths, and the fractional composition (Tables 6 and 7) of the excited states. *m*PW1PW91 shows a similar trend that is accompanied by a shift to higher energies for almost all main excitations (Table 8). The exchange-correlation of the BLYP pure functional contains a local generalized gradient approximation (GGA), and provides significantly different excitation energies, oscillator strengths and a composition from previous hybrid functional (Table 9). The root-mean-square (RMS) of BLYP in the excitation energy represents a minimum (0.220 eV). The B3LYP and B3P86 functionals led to very good similar results for the excitation energy (i.e., 0.306 eV for B3LYP and 0.290 eV for B3P86).

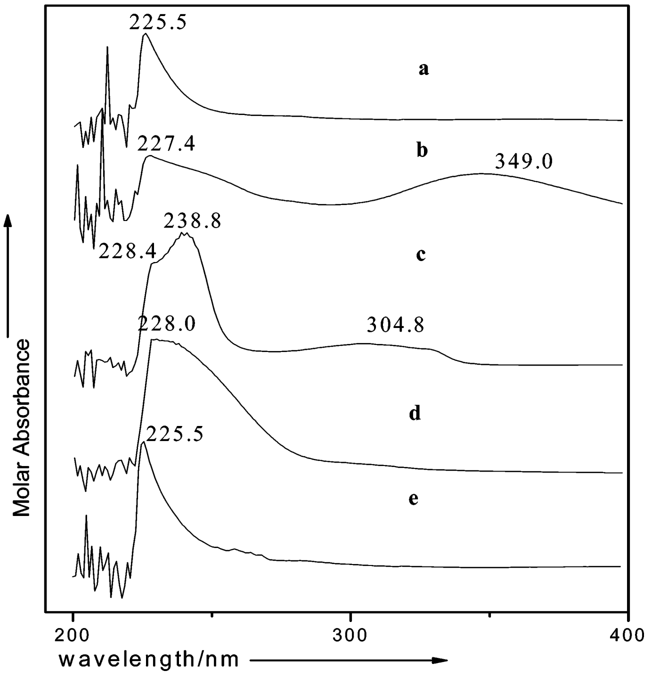

Figure 4. The UV−vis absorption spectra of compounds **a**, **b**, **c**, **d**, and **e**.

TABLE 5: Computed Vertical Excitation Energy (in eV) and Oscillator Strengths (in Parentheses) with Different Exchange-Correlation Functionals in Comparison to Experiment

exp.	B3LYP /6-31G(d)	B3P86 /6-31G(d)	*m*PW1PW91 /6-31G(d)	BLYP /6-31G(d)
		Compound a		
5.50 (225.5)	5.29 (234.2)	5.53 (224.4)	5.55(223.4)	5.19(239.0)
		Compound b		
5.45 (227.4)	5.65(219.5)	5.64(220.0)	5.32(233.1)	5.09(243.6)
3.55(349.0)	3.77 (329.1)	3.78(327.8)	3.84(323.1)	3.88(319.4)
		Compound c		
4.07 (304.8)	4.78(259.2)	4.74(261.7)	4.96(250.2)	3.94(315.1)
5.19 (238.8)	5.03(246.4)	5.01(247.6)	5.29(234.2)	5.17(239.7)
5.43(228.4)	5.35(231.6)	5.35(231.7)	5.51(225.0)	5.32(233.1)
		Compound d		
5.44 (228.0)	5.49(226.0)	5.50(225.6)	5.67(218.6)	5.44 (227.7)
		Compound e		
5.50(225.5)	5.78(214.4)	5.80(213.8)	5.55(223.4)	5.35(231.6)

TABLE 6: Computed Vertical Excitation Energy (eV), Oscillator Strengths, and Fraction Composition for the Optically Allowed Excited States at B3LYP/6-31G(d) Level[a]

states	composition	excitation energy (eV)	wavelength (nm)	oscillator strength
		Compound a		
5^1A	H−0→L+2(+48%) H−1→L+0(28%) H−1→L+1 (+12%)	5.29	234.2	0.0199
		Compound b		
6 ^{1}A	H−6→L+0(+34%) H−6→L+1(16%) H−11→L+0(+10%) H−11→L+1(6%)	3.77	329.1	0.0110
24 ^{1}A	H−8→L+1(+47%) H−1→L+2(8%) H−11→L+0(+6%) H−13→L+0 (6%)	5.10	243.2	0.1042
34 ^{1}A	H−1→L+4(+66%) H−0→L+4(+20%)	5.65	219.5	0.0261
		Compound c		
1 ^{1}A	H−0→L+0(+96%)	4.78	259.2	0.0205
2 ^{1}A	H−0→L+1(+96%)	4.87	254.4	0.0139
3^1A	H−0→L+2(+99%)	5.03	246.4	0.0210
4 ^{1}A	H−1→L+2(+65%) H−1→L+3(+13%) H−1→L+0(6%)	5.35	231.6	0.0025
		Compound d		
1^1A	H−1→L+0(+50%) H−1→L+3(27%) H−1→L+2(+7%)	4.98	248.8	0.0145
8 ^{1}A	H−2→L+1(+35%) H−3→L+0(29%) H−1→L+1(14%) H−3→L+1(+7%)	5.49	226.0	0.0182
		Compound e		
5 ^{1}A	H−1→L+1(+35%) H−5→L+0(20%) H−1→L+0(+18%) H−3→L+0(12%) H−3→L+1(6%)	5.78	214.4	0.0024

[a] H, HOMO (highest occupied molecular orbital); L, LUMO (lowest unoccupied molecular orbital).

TABLE 7: Computed Vertical Excitation Energy (eV), Oscillator Strengths, and Fraction Composition for the Optically Allowed Excited States at B3P86/6-31G(d) Level[a]

states	composition	excitation energy (eV)	wavelength (nm)	oscillator strength
	Compound a			
5 ^{1}A	H−0→L+2(+58%)	5.53	224.4	0.0069
	H−0→L+1(+19%)			
	H−0→L+4(+9%)			
	H−0→L+3(7%)			
	Compound b			
6^{1}A	H−6→L+0(+32%)	3.78	327.8	0.0107
	H−6→L+1(+15%)			
	H−11→L+0(7%)			
	H−3→L+0(+7%)			
	H−10→L+0(5%)			
24 ^{1}A	H−8→L+1(+47%)	5.11	242.6	0.1084
	H−1→L+2(+6%)			
	H−11→L+0(+6%)			
	H−13→L+0(+5%)			
34 ^{1}A	H−1→L+4(+72%)	5.64	220.0	0.0303
	H−0→L+4(+12%)			
	Compound c			
1 ^{1}A	H−0→L+0(+96%)	4.74	261.7	0.0210
2 ^{1}A	H−0→L+1(+97%)	4.83	256.6	0.0140
3 ^{1}A	H−0→L+2(+99%)	5.01	247.6	0.0217
4 ^{1}A	H−1→L+2(+71%)	5.35	231.7	0.0025
	H−1→L+3(10%)			
	H−1→L+0(7%)			
	Compound d			
1 ^{1}A	H−1→L+0(+57%)	4.97	249.4	0.0155
	H−1→L+3(24%)			
	H−1→L+2(+6%)			
8 ^{1}A	H−2→L+1(+37%)	5.50	225.6	0.0173
	H−3→L+0(31%)			
	H−1→L+1(8%)			
	H−3→L+1(+8%)			
	H−2→L+0 (+6%)			
	Compound e			
5 ^{1}A	H−1→L+1(+36%)	5.80	213.8	0.0024
	H−5→L+0(20%)			
	H−1→L+0(+18%)			
	H−3→L+0(13%)			
	H−3→L+1(6%)			

[a] H, HOMO (highest occupied molecular orbital); L, LUMO (lowest unoccupied molecular orbital).

TABLE 8: Computed Vertical Excitation Energy (eV), Oscillator Strengths, and Fraction Composition for the Optically Allowed Excited States at *m*PW1PW91/6-31G(d) Level[a]

states	composition	excitation energy (eV)	wavelength (nm)	oscillator strength
	Compound a			
5 ^{1}A	H−0→L+2(+70%)	5.55	223.4	0.0168
	H−1→L+0(18%)			
	Compound b			
5 ^{1}A	H−6→L+0(+27%)	3.84	323.1	0.0115
	H−6→L+1(+16%)			
	H−11→L+0(+12%)			
	H−11→L+1(+9%)			
	H−9→L+0(+7%)			
24^{1}A	H−7→L+1(+51%)	5.32	233.1	0.0938
	H−1→L+2(+8%)			
29 ^{1}A	H−1→L+4(+29%)	5.74	216.1	0.0309
	H−0→L+4(20%)			
	H−1→L+3(16%)			
	H−2→L+2(6%)			
	Compound c			
1 ^{1}A	H−0→L+0(+93%)	4.96	250.2	0.0269
2 1A	H−0→L+1(+93%)	5.07	244.5	0.0097
3 ^{1}A	H−0→L+2(+98%)	5.29	234.2	0.0229
4 ^{1}A	H−1→L+2(+24%)	5.51	225.0	0.0031
	H−5→L+2(22%)			
	H−6→L+2(18%)			
	H−7→L+2(13%)			
	H−1→L+3(10%)			
	Compound d			
1^{1}A	H−1→L+3(39%)	5.11	242.7	0.0120
	H−1→L+0(+37%)			
	H−1→L+2(+8%)			
	H−5→L+3(5%)			
8 ^{1}A	H−1→L+1(+55%)	5.67	218.6	0.0265
	H−2→L+1(19%)			
	H−3→L+0(+11%)			
	Compound e			
3 ^{1}A	H−1→L+1(+46%)	5.55	223.4	0.0019
	H−3→L+0(+26%)			
	H−0→L+1(7%)			

[a] H, HOMO (highest occupied molecular orbital); L, LUMO (lowest unoccupied molecular orbital).

The *m*PW1PW91 produces significant errors and its RMS is 0.350 eV.

For compound **a**, the only strong band was attributed to the 5^{1}A excited state and it is due to two transitions: the H−0→L+2 (48%, B3LYP; 58%, B3P86; 70%, *m*PW1PW91) and the H−1→L+0 configurations (28%, B3LYP; 19%, B3P86; 18%, *m*PW1PW91). The 5^{1}A excited-state calculated according to the B3P86 functional lies at 5.53 eV (224.4 nm), which is the best agreement with the experimental data (5.50 eV, 225.5 nm). *m*PW1PW91 also offers a good description of this excitation energy (5.55 eV, 223.4 nm). However, both, the B3LYP (5.29 eV, 234.2 nm) and the BLYP (5.19 eV, 239.0 nm) functionals underestimate the experimental values.

The UV−vis absorption spectrum of compound **b** mainly consists of a strong broad band lying at 227.4 nm and a broad band at 349.0 nm. According to the B3LYP and the B3P86 functionals, the excited state to which we can assign the band at 349.0 nm is a 6^{1}A excited state. It arises from the following transitions: the H−6→L+0 and the H−6→L+1 configurations. They are located at 3.77 (329.1 nm, B3LYP) and 3.78 eV (327.8 nm, B3P86), respectively. According to the *m*PW1PW91 calculation results, the 5^{1}A (3.84 eV, 323.1 nm) excited state can be assigned to this band. Actually, all hybrid and pure functionals overestimate the experimental value. The other peak at 227.4 nm is an overlapping broad strong band. It was attributed to the 24^{1}A and the 34^{1}A excited states. The 24^{1}A excited state lies at 5.10 eV (243.2 nm, B3LYP) and is mainly formed by the H−8→L+1 transition. The 34^{1}A excited state is located at 5.65 eV (219.5 nm, B3LYP) and is given by the following two transitions: the H−1→L+4 and the H−0→L+4 configurations. Both B3LYP and B3P86 overestimate the experimental values by about 0.2 eV, while the BLYP functional led to a discrepancy of about 0.36 eV. The *m*PW1PW91 is in good agreement with the experiment.

The UV−vis absorption spectrum for compound **c** consists of a strong overlapping band and a weak broad band, which are located at 4.07 (304.8 nm), 5.19 (238.8 nm), and 5.43 eV (228.4 nm), respectively. Based on the BLYP calculation results, the broad peak was attributed to the nearer two excited states: 2^{1}A and 3^{1}A, respectively. They have comparable excitation energies and oscillator strengths, i.e., 3.91 eV (0.0178) for 2^{1}A and 3.91 eV (0.0284) for 3^{1}A, respectively. The 2^{1}A excited state is mainly formed by the follwing transition: H−0→L+1 configuration, while the 3^{1}A excited state is given by the H−0→L+2 configuration. Based on the B3LYP, B3P86, and

TABLE 9: Computed Vertical Excitation Energy (eV), Oscillator Strengths, and Fraction Composition for the Optically Allowed Excited States at BLYP/6-31G(d) Level[a]

states	composition	excitation energy (eV)	wavelength (nm)	oscillator strength
	Compound a			
18 ^{1}A	H−1→L+5(+39%) H−3→L+0(+35%) H−2→L+1(+14%**)**	5.19	239.0	0.0180
	Compound b			
19^{1}A	H−9→L+0(+64%) H−8→L+0(9%) H−8→L+1(+7%	3.88	319.4	0.0131
36^{1}A	H−11→L+1(+26%) H−12→L+1(+22%) H−9→L+1(+8%) H−10→L+1(6%)	4.65	266.8	0.1972
44 ^{1}A	H−3→L+3(+53%) H−3→L+4(+22%) H−4→L+3(+19%)	5.09	243.6	0.0033
	Compound c			
2 ^{1}A	H−0→L+1(66%) H−0→L+0(24%) H−0→L+2(+6%)	3.91	317.3	0.0178
3 ^{1}A	H−0→L+2 (+92%)	3.94	315.1	0.0284
18 ^{1}A	H−5→L+2(+63%) H−4→L+2(22%) H−5→L+0(9%)	5.17	239.7	0.0055
22^{1}A	H−1→L+4(+96%)	5.32	233.1	0.0029
	Compound d			
10 ^{1}A	H−2→L+0(+64%) H−3→L+0(+15%) H−1→L+4(+14%)	4.89	253.5	0.0136
22 ^{1}A	H−2→L+3(+74%)	5.44	227.7	0.0342
	Compound e			
10 ^{1}A	H−4→L+0(+72%) H−1→L+2(+25%)	5.35	231.6	0.0015

[a] H, HOMO (highest occupied molecular orbital); L, LUMO (lowest unoccupied molecular orbital).

*m*PW1PW91 calculations, the 1^{1}A (4.78 eV, B3LYP; 4.74 eV, B3P86; 4.96 eV, *m*PW1PW91) and the 2^{1}A (4.87 eV, B3LYP; 4.83 eV, B3P86; 5.07 eV, *m*PW1PW91) excited states were assigned to this band. All hybrid functionals overestimate the experimental value greatly (about 0.7 eV). The bands at 238.8 nm (5.19 eV) and 228.4 nm (5.43 eV) can be attributed to the 18^{1}A (5.17 eV, 239.7 nm) and 22^{1}A (5.32 eV, 233.1 nm) excited states, which are due to the H−5→L+2 and H−1→L+4 transitions, respectively. All hybrid functionals give a good description of these two excitation energies (i.e., 5.03 and 5.35 eV by using B3LYP; 5.01 and 5.35 eV by using B3P86; 5.29 and 5.51 eV by using *m*PW1PW91).

The strong broad peak located at 5.50 eV (225.5 nm) in the UV−vis spectrum of **d** was attributed to the 1^{1}A and 8^{1}A excited states for all functionals. The B3LYP (4.98 eV, 248.8 nm; 5.49 eV, 226.0 nm), B3P86 (4.97 eV, 249.4 nm; 5.50 eV, 225.6 nm), and BLYP (4.89 eV, 253.5 nm; 5.44 eV, 227.7 nm) functionals reproduced this absorption band very well. However, *m*PW1PW91 (5.11 eV (242.7 nm), 5.67 eV (218.6 nm)) overestimated the experimental value.

The UV−vis absorption spectrum of compound **e** consists of a single band at 225.5 nm. According to the B3LYP and the B3P86 functionals, it was ascribed to the 5^{1}A excited state and was found to be due to the following two transitions: H−1→L+1 and H−5→L+0 configurations. They are located at 5.78 (214.4 nm, B3LYP) and 5.80 eV (213.8 nm, B3P86), respectively. *m*PW1PW91 (5.55 eV, 223.4 nm) describes very well the excitation energy.

According to the population analysis for the compounds **a**−**e**, the strong bands near 226.0 nm mainly arise from the $n \rightarrow \pi^*$ transition of the amide. The transannular effect determines a strong absorption and a significant red shift of its maximum absorption wavelength. Due to the large conjugation of the lone pair electron of the nitrogen atom and the conjugated π system of the nitrobenzene, the maximum absorption wavelength of the $\pi \rightarrow \pi^*$ transition shifts to 349.0 nm for compound **b**.

4. Conclusion

The FT-Raman and UV−vis absorption spectra of five derivates of (12S)-1,4,7,10-tetraazadicyclo[10,3,0]-pentadecane-3,11-dione were recorded and discussed. Their geometries and harmonic vibrational wavenumbers were determined by performing DFT calculations at the B3LYP/6-31G(d) level of theory. The calculated wavenumbers were then scaled and compared with the experimental values. The discrepancies were mostly <30 cm^{-1}. Compound **b** was found to have an amide (II) character, while the others compounds have an amide (I) character. The dinitrobenzene insertion at C1 lowers the HOMO and LUMO energy levels drastically for compound **b** in comparison with those of the other compounds. Moreover, the different substituents do not cause a significant shift of the vibrational mode of the macrocyclic plane. The dimolecular model proved that strong inter- and intramolecular hydrogen bonds are present in these compounds. The electronic vertical excitation energies and the oscillator strengths were determined with the help of TDDFT calculations and by employing pure (BLYP) and hybrid (B3LYP, B3P86, and *m*PW1PW91) functionals together with the 6-31G(d) basis set. The BLYP functional describes the excitation energies better than the B3LYP, B3P86, or *m*PW1PW91 hybrid functionals. Due to the transannular effect, the UV−vis absorption spectrum of macrocyclic dioxotetraamines becomes abnormal. The $n \rightarrow \pi^*$ transitions of the amide determines a very strong absorption and a shift toward longer wavelengths.

Acknowledgment. Financial support from the National Natural Science Foundation of China and the Deutsche Forschungsgemeinschaft is highly acknowledged. Contract/grant sponsor: National Natural Science Foundation of China; Contract/grant number: 20375029, 20211130525 and 20411130312. Contract/grant sponsor: Deutsche Forschungsgemeinschaft 446 CHV-112/52/02 and 446 CHV-112/12/04. W.K. and I.P. thank the Founds der Chemischen Industrie for financial support.

References and Notes

(1) Kodama, M.; Kimura, E. *J. Chem. Soc., Dalton Trans.* **1981**, 694.
(2) Kodama, M.; Kimura, E. *J. Chem. Soc., Dalton Trans.* **1979**, 325.
(3) Kimura, E.; Yatsunami, T.; Watanabe, A.; Michida, T.; Koike, T.; Fujioka, H.; Kuramoto, Y.; Sumomogi, M.; Kunimitsu, K.; Yamashita, A. *Biochim. Biophys. Acta* **1983**, *37*, 745.
(4) Machida, R.; Kimura, E.; Kodama, M. *Inorg. Chem.* **1983**, *22*, 2055.
(5) Shionoya, M.; Ikeda, T.; Kimura, E. *J. Am. Chem. Soc.* **1994**, *116*, 3848.
(6) *Progress in Inorganic Chemistry*, Kimura, E., Ed.; John Wiley& Sons: New York, 1994; p 443.
(7) Zhu, S. R.; Lin, H. K.; Lin, C. C.; Kou, F. P.; Chen, Y. T. *Inorg. Chim. Acta* **1995**, *228*, 225.
(8) Bu, X. H.; Zhang, Z. H.; Cao, X. C.; Ma, S. Y.; Chen, Y. T. *Polyhedron* **1997**, *16*, 3525.
(9) Zhang, Z. H.; Bu, X. H.; Cao, X. C.; Wang, C. Z.; Chen R. T. *Chin. J. Struct. Chem.* **1999**, *18*, 14.
(10) An, D. L.; Bu, X. H.; Lin, H. K.; Liu, Y.; Chen, Y. T. *Chin. Chem. Lett.* **1994**, *5*, 537.
(11) Jia, D. F.; Lin, M. R.; Fang, F.; Zhu, S. R. *J. Tianjin Univ.* **2001**, *34*, 368.
(12) Jia, D. F.; Lin, M. R.; Fang, F.; Zhu, S. R. *Spectrosc. Spectral Analys.* **2002**, *22*, 99.

(13) Lampeka, Y. D.; Gavrish, S. P. *Polyhedron* **2000**, *19*, 2533.

(14) Kodama, M.; Anan, H.; Koike, T.; Kimura, E. *Bull. Chem. Soc. Jpn.* **1989**, *62*, 4044.

(15) Kodama, M.; Kimura, E. *Bull. Chem. Soc. Jpn.* **1989**, *62*, 3039.

(16) Runge, E.; Gross, E. K. U. *Phys. Rev. Lett.* **1984**, *52*, 997.

(17) Petersilka, M.; Gossmann, U. J.; Gross, E. K. U. *Phys. Rev. Lett.* **1996**, *76*, 1212.

(18) Cavillot, V.; Champagne, B. *Chem. Phys. Lett.* **2002**, *354*, 449.

(19) Hirata, S.; Gordon, M. H.; Szczepanski, J.; Vala, M. *J. Phys. Chem. A* **2003**, *107*, 4940.

(20) Van Gisbergen, S. J. A.; Rosa, A.; Ricciardi, G.; Baerends, E. J. *J. Chem. Phys.* **1999**, *111*, 2499.

(21) Yuan, Q.; Xue, P.; Fang, M. H.; Fu, E. Q.; Wu, C. T. *Synth. Commun.* **2003**, *33*, 1911.

(22) Yuan, Q.; Fu, E. Q.; Wu, X. J.; Fang, M. H.; Xue, P.; Wu, C. T.; Chen, J. H. *Tetrahedron Lett.* **2002**, *43*, 3935.

(23) Frisch, M. J.; Trucks, G. W.; Schlegel, H. B.; Scuseria, G. E.; Robb, M. A.; Cheeseman, J. R.; Zakrzewski, V. G.; Montgomery, J. A., Jr.; Stratmann, R. E.; Burant, J. C.; Dapprich, S.; Millam, J. M.; Daniels, A. D.; Kudin, K. N.; Strain, M. C.; Farkas, O.; Tomasi, J.; Barone, V.; Cossi, M.; Cammi, R.; Mennucci, B.; Pomelli, C.; Adamo, C.; Clifford, S.; Ochterski, J.; Petersson, G. A.; Ayala, P. Y.; Cui, Q.; Morokuma, K.; Malick, D. K.; Rabuck, A. D.; Raghavachari, K.; Foresman, J. B.; Cioslowski, J.; Ortiz, J. V.; Stefanov, B. B.; Liu, G.; Liashenko, A.; Piskorz, P.; Komaromi, I.; Gomperts, R.; Martin, R. L.; Fox, D. J.; Keith, T.; Al-Laham, M. A.; Peng, C. Y.; Nanayakkara, A.; Gonzalez, C.; Challacombe, M.; Gill, P. M. W.; Johnson, B. G.; Chen, W.; Wong, M. W.; Andres, J. L.; Head-Gordon, M.; Replogle, E. S.; Pople, J. A. *Gaussian 98*; Gaussian, Inc.: Pittsburgh, PA, 1998.

(24) Scott, A. P.; Radom, L *J. Phys. Chem.* **1996**, *100*, 16502.